Materials Transactions, Vol. 62, No. 8 (2021) pp. 1225 to 1230

Reduction of Spatter Generation Using Atmospheric Gas in Laser Powder Bed Fusion of Ti–6Al–4V

Hiroki Amano[1,2,*1], Yusuke Yamaguchi[2], Takuya Ishimoto[1] and Takayoshi Nakano[1,*2]

[1]*Division of Materials and Manufacturing Science, Graduate School of Engineering, Osaka University, Suita 565-0871, Japan*
[2]*TAIYO NIPPON SANSO Corporation, Tokyo 142-8558, Japan*

Laser powder bed fusion (LPBF), a typical additive manufacturing (AM) process, is a promising approach that enables high-accuracy manufacturing of arbitrary structures; therefore, it has been utilized in the aerospace and medical fields. However, several unexplained phenomena significantly affect the quality of fabricated components. In particular, it has been reported that the generation of spatters adversely affects the stability of fabrication process and degrades the performance of the fabricated components. To realize high-quality components, it is essential to suppress the generation of spatters. Thus far, the suppression of spatter generation has been attempted based on the process parameters; however, this has not been adequately discussed in terms of the fabrication atmosphere. Therefore, in this study, we focused on the fabrication atmosphere and investigated spatter generation using gas with different physical properties rather than conventionally used argon. It was observed that the spatter generation during the fabrication of the Ti–6Al–4V alloy could be significantly suppressed by changing the atmospheric gas, even under constant LPBF process parameters. We proved that the fabrication atmosphere is an important factor to be considered, apart from the process parameters, in AM technology. [doi:10.2320/matertrans.MT-M2021059]

(Received March 26, 2021; Accepted April 30, 2021; Published June 11, 2021)

Keywords: *laser powder bed fusion, titanium alloy, biomaterials, spatter, atmosphere, gas*

1. Introduction

Additive manufacturing (AM) is a metal processing technology that enables the high-precision manufacturing of structures with arbitrary shapes.[1–4] Recently, the laser powder bed fusion (LPBF) method, a type of AM technology, has attracted attention as a process capable of controlling not only the shape of metallic materials but also their crystallographic textures[5–14] and related mechanical and chemical functions.[5,7,12]

However, defects can be formed during fabrication, which, in turn, deteriorates the properties of the components, induces uncertainty in the quality control of components, and consequently, hinders the practical application of AM in various industries.[15] The generation of spatters is proven to be one of the main causes of defect formation.[16,17] Figure 1 shows spatter generation during LPBF fabrication. Spatter generation has been reported to reduce the energy efficiency of the laser owing to the spatter passing through the optical path of the laser.[18–20] Moreover, the material properties of the fabricated components are affected by the incorporation of spatter particles.[21] The unmelted powder in LPBF is typically reused; however, the spatter contained in the unmelted powder may affect the subsequent fabrication process. For example, there is a risk of unexpected elevation in the oxygen concentration in the fabricated components. Therefore, it is essential to reduce spatter generation to ensure the quality control of the components fabricated using LPBF. Recent studies have attempted to control spatter generation using the process parameters in LPBF. It has been reported that spatter generation is reduced by lowering the laser output or increasing the laser scanning speed[22] and using the pulse oscillations of the laser rather than continuous oscillations.[23] However, an optimal range of process parameters to achieve the desired microstructures and suppress spatter generation do not necessarily match. Therefore, it is important to suppress spatter generation by utilizing atmospheric gas, rather than the process parameters, during fabrication.

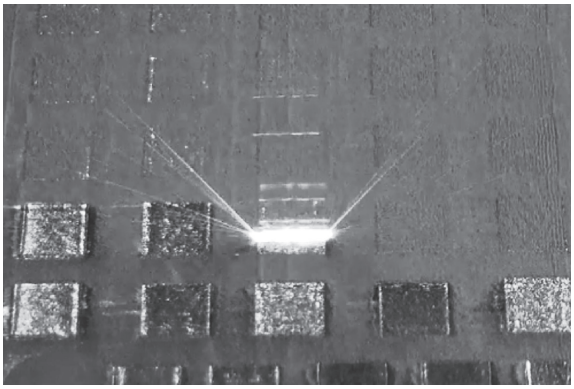

Fig. 1 Still image of spatter generation at the time of LPBF fabrication.

In general, argon or nitrogen is used as the atmospheric gas in LPBF. The Ti–6Al–4V alloy has high strength, corrosion resistance, and high-temperature properties, such as creep strength, and is used in a wide range of fields;[24,25] however, it is a highly reactive metal. As it reacts with nitrogen at high temperatures, argon is generally chosen as the atmospheric gas in the LPBF. There is no significant difference in the thermal conductivities or densities between argon and nitrogen; however, these gases show different reactivities with metals. As an inert gas, helium can be considered as an alternative to argon. As presented in Table 1, helium has significantly different properties compared to argon, such as a density of approximately 0.1 times and thermal conductivity of approximately 10 times that of argon; it also exhibits excellent cooling properties.[26] In other words, the atmospheric gas is capable of cooling in addition to its reactivity with metals. However, very few studies have focused on the use of atmospheric gases in LPBF.

*[1]Graduate Student, Osaka University
*[2]Corresponding author, E-mail: nakano@mat.eng.osaka-u.ac.jp

Table 1 Gas properties of argon and helium (standard ambient temperature and pressure).[26)]

	Argon	Helium
Molecular weight, M/kg·mol^{-1}	39.96	4.003
Density, ρ/kg·m^{-3}	1.6339	0.16353
Thermal conductivity, λ/mW·m^{-1}K^{-1}	17.746	155.31
Viscosity, μ/μPa·s	22.624	19.846
Heat capacity, C_p/kJ·kg^{-1}K^{-1}	0.52156	5.193

Furthermore, there are several unexplained phenomena regarding spatter generation and the atmosphere, a control method for which is yet to be established.

In this study, we focused on the fabrication atmosphere of LPBF and investigated its effect on spatter generation using helium. This research is expected to improve the quality of the fabricated components and promote the reuse of powder, leading to an improvement in the applicability of LPBF.

2. Experimental Procedure

The LPBF process is typically conducted using an inert atmospheric gas to prevent the contamination of the fabricated components. In this study, we focused on helium gas and investigated the effect of oxygen as an impurity in the atmosphere. To analyze the spatter generation behavior under atmospheric gas, we developed a basic evaluation equipment for single-layer fabrication using the LPBF method. We conducted a laser irradiation experiment on a powder bed. Ti–6Al–4V ELI alloy powder (Al: 6.5, C: 0.01, Fe: 0.2, H: 0.002, N: 0.02, O: 0.12, V: 4.1, and Ti: bal. (mass%)) with a particle size of less than 53 μm was used in this experiment.

Figure 2 demonstrates a schematic ((a) system diagram and (b) structure diagram) of the basic evaluation equipment for the single-layer fabrication used in this experiment. This equipment includes a laser oscillator (red POWER; SPI Lasers, UK), galvanometer mirror (Canon) and mass flow controller (MQV series; Azbil). Dew point meter (DM70; Vaisala, Finland) and oxygen analyzer (3300TA; Teledyne, Japan) were used to monitor the atmosphere in the experimental chamber.

As shown in Fig. 3(a), a 30 μm thick metal foil with a cut-out in the center was placed on a pure Ti base plate, and the metal powder was placed in the cut-out area. Then, by moving the recoater in one direction, a Ti–6Al–4V powder bed with a layer thickness of 30 μm was formed and placed in the basic evaluation equipment for single-layer fabrication. The atmosphere inside the chamber comprised helium gas with a controlled oxygen concentration at a constant flow rate, achieved using the mass flow controller. After the atmosphere was stabilized, the laser was irradiated over the powder bed on the base plate. The laser irradiation conditions were as follows: a laser power of 200 W, scanning speed of 800 mm/s, laser spot diameter of 50 μm, scan pitch of 50 μm, and laser irradiation region of 15 mm × 15 mm (Fig. 3(b)). In addition, the experiment was conducted in an argon atmosphere under the same laser irradiation conditions for comparison. The spatter generation behaviors during laser irradiation of the two gases were recorded using a video recorder.

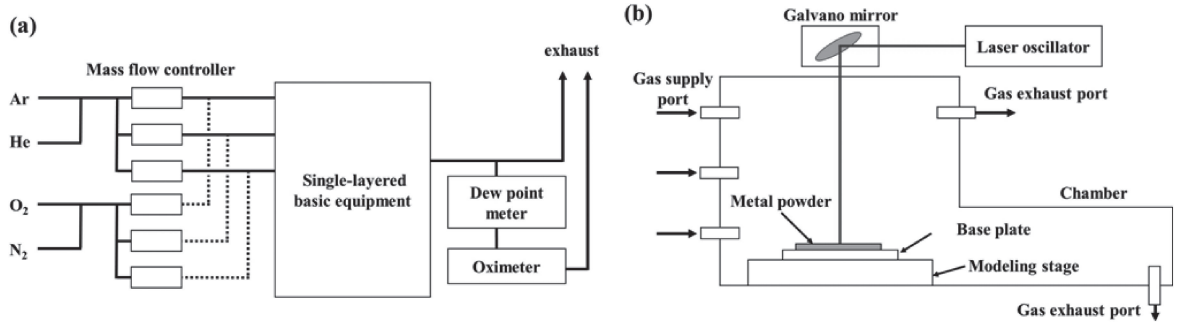

Fig. 2 Schematic of the basic evaluation equipment for single-layer fabrication ((a) system diagram and (b) structure diagram).

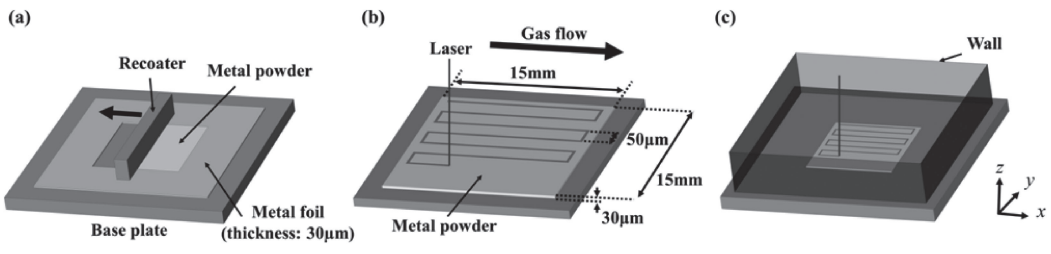

Fig. 3 Schematic of (a) 30 μm powder bed formation, (b) laser irradiation pattern, and (c) spatter collection wall.

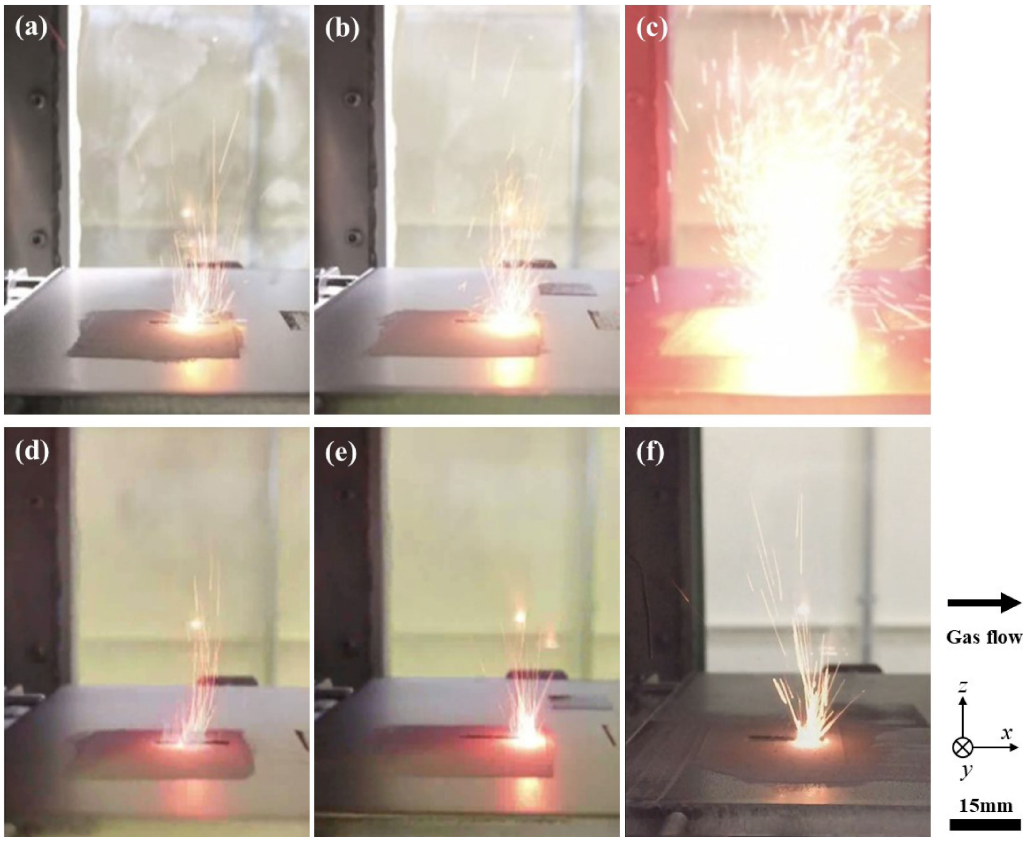

Fig. 4 Still images at the time of spatter generation in (a)–(c) argon and (d)–(f) helium atmospheres ((a) and (d) <50 vol. ppm O_2, (b) and (e) 1.0 vol% O_2, and (c) and (f) 5.0 vol% O_2).

To evaluate the spatters generated during laser irradiation, a wall was placed on the base plate such that all the spatters remained on the base plate (Fig. 3(c)). All powders on the base plate were recovered; they comprised unmelted powder and spatters. To remove the unmelted powder, the collected powder was sieved through an open mesh of 53 µm; thus, powders with a particle diameter of 53 µm or more were recovered and treated as spatters. The recovered spatters were then subjected to morphological observations using field-emission scanning electron microscopy (FE-SEM).

3. Results and Discussion

The spatter generation behaviors during laser irradiation were evaluated to determine the difference in the amount of spatter generated under the two atmospheric gas species. Figures 4(a) and (d) depict still images representing spatter generation under argon and helium gases. Figure 5 presents the weights of generated spatter. The amount of spatter generated under helium was less than that generated under argon. Note that the effect of oxygen concentration will be discussed later. There was no difference in the appearance of the spatter particles depending on the atmospheric gas species, as shown in Fig. 6.

The decreased spatter generation when helium was used might be attributed to the thermal conductivity and density of helium. As presented in Table 1, helium shows approximately 10 times higher thermal conductivity and density of approximately 1/10 times compared to that of argon. The thermal conductivity affected the cooling rate during solidification. Here, the heat transfer coefficient between the fabricated component and the gas phase (argon or helium) in the laser irradiation region was calculated. The heat transfer coefficient can be expressed using the following equation:[27]

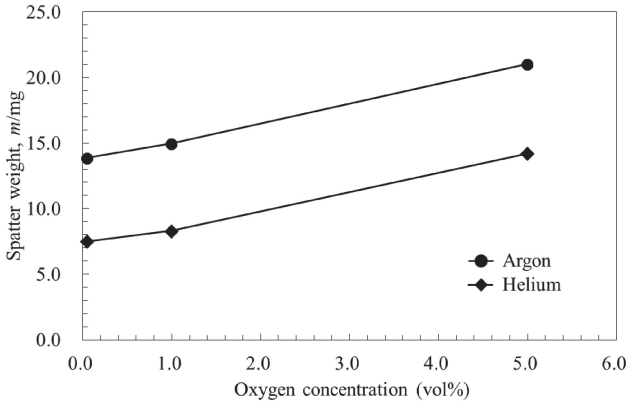

Fig. 5 Variation in generated spatter weight under argon and helium atmospheres.

$$Re = \rho V l/\mu, \tag{1}$$

$$Pr = \mu C_p/\lambda, \tag{2}$$

$$Nu = 0.664 Re^{1/2} Pr^{1/3}, \tag{3}$$

$$Nu = hl/\lambda, \tag{4}$$

where Re denotes the Reynolds number, ρ denotes the fluid density, V denotes the fluid velocity, l denotes the representative length, μ denotes the absolute viscosity, Pr

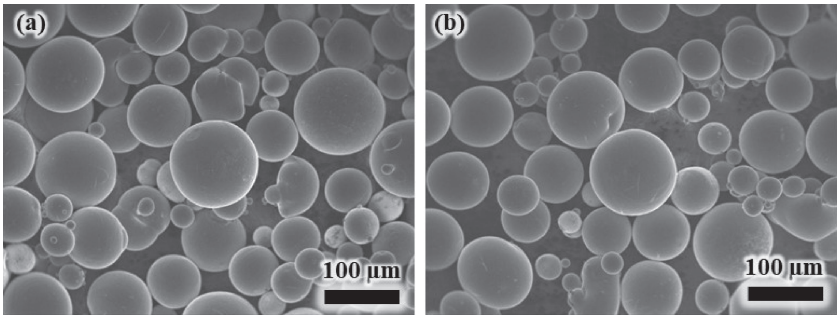

Fig. 6 FE-SEM images of spatters generated during fabrication in (a) argon and (b) helium atmospheres (<50 vol. ppm O_2).

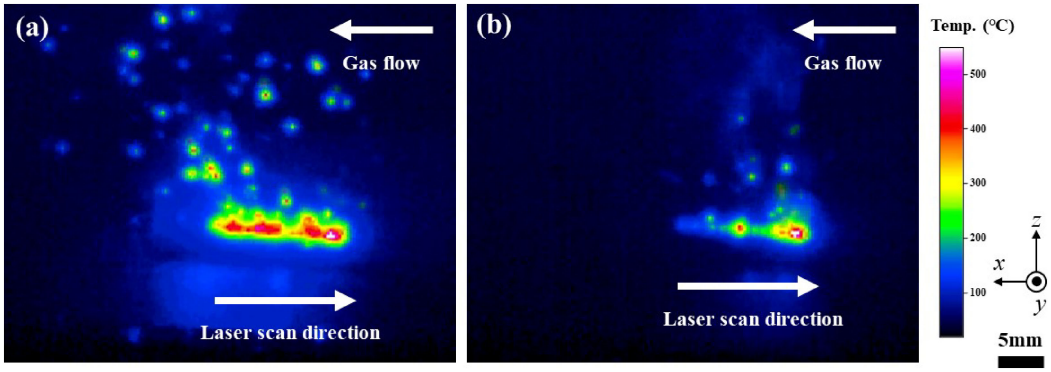

Fig. 7 Thermal images of spatter generation in (a) argon and (b) helium atmospheres (<50 vol. ppm O_2).

denotes the Prandtl number, λ denotes the thermal conductivity, C_p denotes the specific heat, Nu denotes the Nusselt number, and h denotes the heat transfer coefficient. When the flow velocity on the base plate was the same for both argon and helium, the heat transfer coefficient using helium was approximately 2.7 times large as that using argon. The higher the heat transfer coefficient, the higher is the cooling rate of the laser irradiation region.[28] Spatter was generated when metal powder was wound up by the expansion of atmospheric gas that was instantaneously heated to a high temperature in the laser irradiation region and the subsequent generation of an updraft.[29] In addition, the reaction pressure owing to the extreme expansion of gas phase generated a spatter of the metal jet.[20] Therefore, the cooling rate increased and the expansion of atmosphere decreased when using helium as compared to that when using argon. Furthermore, as the force acting from the fluid to the material is proportional to the density of the fluid and the density of helium is considerably lower than that of argon, the use of helium could reduce the force acting on the metal powder compared to the use of argon, thereby reducing the amount of spatter generation. The temperature difference at the base plate was observed via thermal imaging (Fig. 7). According to Fig. 7, the region showing high temperature in the base plate is reduced under the use of helium compared to that of argon. In addition, spatter generation in the laser irradiation region was suppressed when helium was used, as represented by the high-speed camera image shown in Fig. 8. This could be attributed to the aforementioned large cooling effect of helium. Such a high cooling rate is also beneficial for the improvement of metallic material function. For example, a high cooling rate significantly enhances the

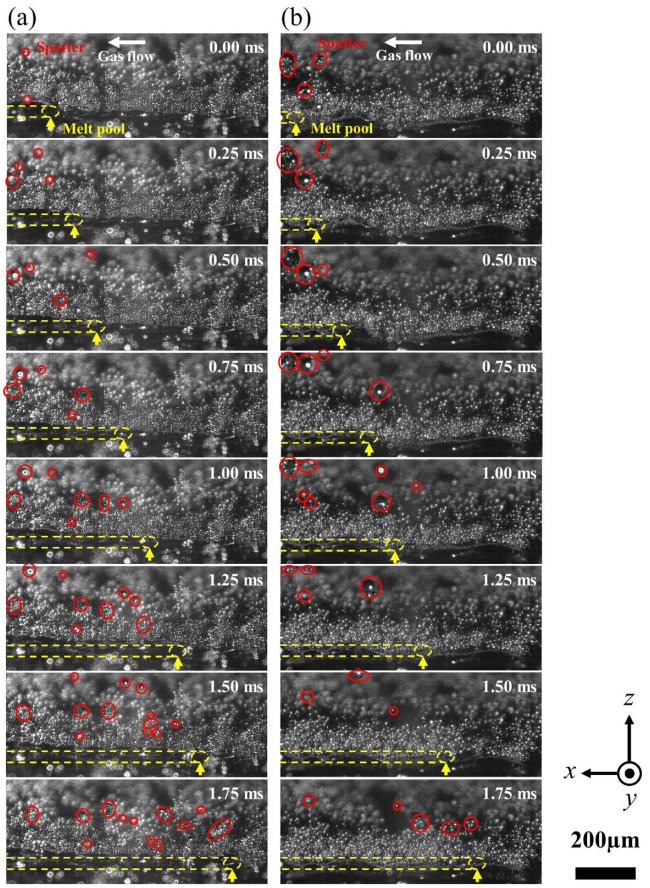

Fig. 8 Still images taken at intervals of 0.25 ms using high-speed camera in (a) argon and (b) helium atmospheres (<50 vol. ppm O_2). The red circle shows the position of the spatters, and the yellow line shows the position of the melt pool and the bead after fabrication.

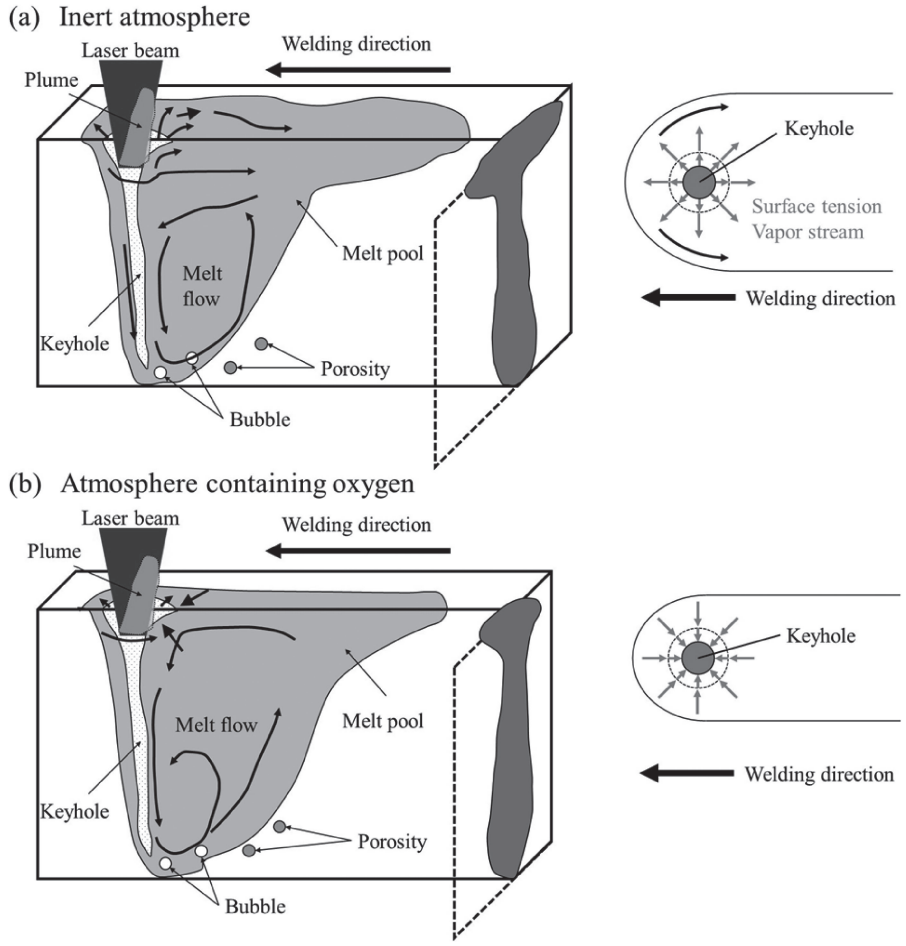

Fig. 9 Schematic of the flow of molten metal in the melt pool during laser welding in (a) inert atmosphere and (b) oxygen containing atmosphere.[32)]

localized corrosion resistance of stainless steel and the mechanical properties of high-entropy alloy by inhibiting the formation and growth of inclusions and achieving super-solid solution formation, respectively.[30,31)]

Next, the effect of oxygen, which is an impurity in atmospheric gas, on spatter generation was investigated. As indicated in Figs. 4 and 5, the amount of spatter increased with the oxygen concentration under both helium and argon atmospheres. For the same oxygen concentration in the atmosphere, the amount of spatter generation was reduced using helium. The increase in amount of spatter with the oxygen concentration was attributed to convection in the melt pool. During laser welding and plasma welding, the flow of molten metal in the melt pool under an inert atmosphere is different from that under an atmosphere containing oxygen. In an inert atmosphere, the surface tension of molten metal decreases with increasing temperature. The surface tension of the molten metal at the melt pool edge becomes higher than that at the melt pool center, which is directly under the laser irradiation, and convection flow occurs from the center toward the edge of the melt pool. Therefore, the molten metal flows from the melt pool center to the rear part of the melt pool, as depicted in Fig. 9(a). However, the surface tension changes in the presence of oxygen. In an atmosphere containing oxygen, the temperature coefficient of surface tension became positive, and the surface tension of the molten metal increased with increasing temperature. Therefore, the direction of convection changed from outward to inward, and the molten metal that was directly under the laser irradiation approached the laser irradiation again, as demonstrated in Fig. 9(b).[32,33)] Thus, the molten metal maintained a high temperature with active flow, which was a suitable condition for spatter generation.

Finally, the spatter generation behavior was evaluated using an actual LPBF apparatus (EOS M 290, EOS, Germany). The oxygen concentration in each atmosphere was set as 0.1 vol%. The spatter generation behavior was found similar (Fig. 10) to the results obtained using the basic evaluation equipment for single-layer fabrication; the spatter generation was suppressed when helium was used.

Based on the abovementioned results, it was evident that atmospheric gas during laser irradiation affected the spatter generation behavior. The use of helium, which enabled a high cooling rate, suppressed spatter generation, unlike the conventionally used argon. Thus, it was shown that during fabrication, the atmospheric gas was another important parameter, apart from the process parameters, which should be considered for the control of spatter generation.

4. Conclusions

In this study, we analyzed spatter generation behaviors

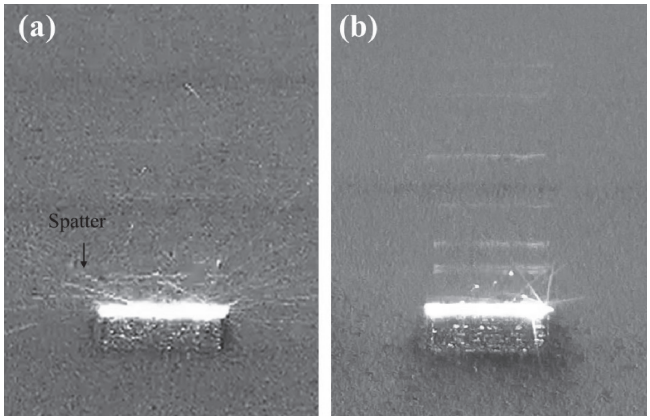

Fig. 10 Still images at the time of spatter generation in (a) argon and (b) helium atmospheres using the LPBF apparatus.

using a basic evaluation equipment for single-layer fabrication using LPBF, to clarify the effect of the atmospheric gas species used in LPBF on spatter generation. The main conclusions of this study are summarized as follows.

(1) The amount of spatter generated when helium was used as the atmospheric gas was less than that when using argon.
(2) With an increase in the oxygen concentration of the atmospheric gas, the amount of spatter increased for both argon and helium atmospheres.
(3) Although the amount of spatter increased with the oxygen concentration in the atmospheric gas, the amount of spatter when using helium was less than that when using argon.

Therefore, it was evident that the atmospheric gas used in LPBF significantly affected the amount of spatter, and the use of helium considerably suppressed spatter generation.

Acknowledgments

This work was supported by Grants-in-Aid for Scientific Research from the Japan Society for the Promotion of Science (JSPS) [grant number JP18H05254]. This work was also partly supported by the Cross-Ministerial Strategic Innovation Promotion Program (SIP) – Materials Integration for Revolutionary Design System of Structural Materials – Domain C1: "Development of Additive Manufacturing Process for Ni-based Alloy" from the Japan Science and Technology Agency (JST).

REFERENCES

1) N. Aage, E. Andreassen, B.S. Lazarov and O. Sigmund: Nature **550** (2017) 84–86.
2) J.H. Zhu, W.H. Zhang and L. Xia: Arch. Comput. Methods Eng. **23** (2016) 595–622.
3) Q. Yan, H. Dong, J. Su, J. Han, B. Song, Q. Wei and Y. Shi: Engineering **4** (2018) 729–742.
4) S. Ghouse, N. Reznikov, O.R. Boughton, S. Babu, K.C.G. Ng, G. Blunn, J.P. Cobb, M.M. Stevens and J.R.T. Jeffers: Appl. Mater. Today **15** (2019) 377–388.
5) T. Ishimoto, K. Hagihara, K. Hisamoto, S.-H. Sun and T. Nakano: Scr. Mater. **132** (2017) 34–38.
6) S.Y. Liu, H.Q. Li, C.X. Qin, R. Zong and X.Y. Fang: Mater. Des. **191** (2020) 108642.
7) T. Boegelein, S.N. Dryepondt, A. Pandey, K. Dawson and G.J. Tatlock: Acta Mater. **87** (2015) 201–215.
8) K. Hagihara, T. Nakano, M. Suzuki, T. Ishimoto, Suyalatu and S.-H. Sun: J. Alloy. Compd. **696** (2017) 67–72.
9) T. Ishimoto, S. Wu, Y. Ito, S.-H. Sun, H. Amano and T. Nakano: ISIJ Int. **60** (2020) 1758–1764.
10) M. Higashi and T. Ozaki: Mater. Des. **191** (2020) 108588.
11) M.S. Pham, B. Dovgyy, P.A. Hooper, C.M. Gourlay and A. Piglione: Nat. Commun. **11** (2020) 749.
12) O. Gokcekaya, N. Hayashi, T. Ishimoto, K. Ueda, T. Narushima and T. Nakano: Addit. Manufact. **36** (2020) 101624.
13) O. Gokcekaya, T. Ishimoto, S. Hibino, J. Yasutomi, T. Narushima and T. Nakano: Acta Mater. **212** (2021) 116876.
14) J. Kubo, Y. Koizumi, T. Ishimoto and T. Nakano: Mater. Trans. (2021) in press.
15) M. Grasso and B.M. Colosimo: Meas. Sci. Technol. **28** (2017) 044005.
16) Y. Liu, Y. Yang, S. Mai, D. Wang and C. Song: Mater. Des. **87** (2015) 797–806.
17) M.J. Zhang, G.Y. Chen, Y. Zhou, S.C. Li and H. Deng: Appl. Surf. Sci. **280** (2013) 868–875.
18) P. Wen, L. Jauer, M. Voshage, Y. Chen, R. Poprawe and J.H. Schleifenbaum: J. Mater. Process. Technol. **258** (2018) 128–137.
19) P. Wen, Y. Qin, Y. Chen, M. Voshage, L. Jauer, R. Poprawe and J.H. Schleifenbaum: J. Mater. Sci. Technol. **35** (2019) 368–376.
20) D. Wang, S. Wu, F. Fu, S. Mai, Y. Yang, Y. Liu and C. Song: Mater. Des. **117** (2017) 121–130.
21) A.B. Anwar and Q.-C. Pham: J. Mater. Process. Technol. **240** (2017) 388–396.
22) V. Gunenthiram, P. Peyre, M. Schneider, M. Dal, F. Coste, I. Koutiri and R. Fabbro: J. Mater. Process. Technol. **251** (2018) 376–386.
23) K. Mumtaz and N. Hopkinson: Rapid Prototyping J. **16** (2010) 248–257.
24) D. Banerjee and J.C. Williams: Acta Mater. **61** (2013) 844–879.
25) M. Geetha, A.K. Singh, R. Asokamani and A.K. Gogia: Prog. Mater. Sci. **54** (2009) 397–425.
26) T.J. Bruno and P.D.N. Svoronos: *CRC Handbook of Basic Tables for Chemical Analysis: Data-Driven Methods and Interpretation*, 4th ed., (CRC Press, Florida, 2020).
27) VDI-Gesellschaft Energietechnik: *Engineering Reference Book on Energy and Heat*, (Springer-Verlag, Berlin, 1992).
28) F.W. Giacobbe: Appl. Therm. Eng. **25** (2005) 205–225.
29) S. Ly, A.M. Rubenchik, S.A. Khairallah, G. Guss and M.J. Matthews: Sci. Rep. **7** (2017) 4085.
30) S.-H. Sun, T. Ishimoto, K. Hagihara, Y. Tsutsumi, T. Hanawa and T. Nakano: Scr. Mater. **159** (2019) 89–93.
31) T. Ishimoto, R. Ozasa, K. Nakano, M. Weinmann, C. Schnitter, M. Stenzel, A. Matsugaki, T. Nagase, T. Matsuzaka, M. Todai, H.S. Kim and T. Nakano: Scr. Mater. **194** (2021) 113658.
32) S. Katayama and Y. Kawahito: J. High Temp. Soc. **33** (2007) 118–127.
33) M.N. Huu, A.N. Van, T.N. Van, D.T. Hai, T.N. Van, D.N. Tien and T.-H. Nguyen: Appl. Sci. **10** (2020) 3569.